J|A|C|S
ARTICLES
Published on Web 04/01/2004

Making a Molecular Wire: Charge and Spin Transport through *para*-Phenylene Oligomers

Emily A. Weiss, Michael J. Ahrens, Louise E. Sinks, Alexey V. Gusev, Mark A. Ratner,* and Michael R. Wasielewski*

Contribution from the Center for Nanofabrication and Molecular Self-Assembly, Department of Chemistry, Northwestern University, Evanston, Illinois 60208-3113

Received November 26, 2003; E-mail: wasielew@chem.northwestern.edu

Abstract: Functional molecular wires are essential for the development of molecular electronics. Charge transport through molecules occurs primarily by means of two mechanisms, coherent superexchange and incoherent charge hopping. Rates of charge transport through molecules in which superexchange dominates decrease approximately exponentially with distance, which precludes using these molecules as effective molecular wires. In contrast, charge transport rates through molecules in which incoherent charge hopping prevails should display nearly distance independent, wirelike behavior. We are now able to determine how each mechanism contributes to the overall charge transport characteristics of a donor−bridge−acceptor (D−B−A) system, where D = phenothiazine (PTZ), B = *p*-oligophenylene, and A = perylene-3,4:9,10-bis(dicarboximide) (PDI), by measuring the interaction between two unpaired spins within the system's charge separated state via magnetic field effects on the yield of radical pair and triplet recombination product.

Introduction

A molecular wire is best understood as a molecular bridge that can move charge rapidly and efficiently over many chemical bond lengths. A major challenge in current chemistry lies in finding molecules that exhibit long-distance charge-transport mechanisms operating with efficiencies found widely in nature. In particular, the photosynthetic reaction center protein rapidly moves electrons with near unity quantum efficiency across a bilayer lipid membrane using several redox cofactors,[1] thus serving as a model for developing synthetic, biomimetic analogues for several applications including solar energy conversion, molecular electronics, and photonic materials.

In assembling electron donor−bridge−acceptor (D−B−A) systems for molecular electronics,[2] one must design the system to adopt the most efficient charge-transport mechanism possible, one which maintains this efficiency as the bridge is lengthened. Long-distance charge transfer (CT) is intrinsically a nonadiabatic process[3,4] in which the CT rate is dictated by some combination of strongly distance-dependent coherent transport and weakly distance-dependent incoherent charge hopping. Optimizing the molecular structure to accentuate the latter process is key to producing wirelike behavior in molecules. To achieve this goal one must (1) isolate the contributions of each mechanism to CT, (2) find the link between these contributions and the energy levels of the system, and (3) choose redox components (donors, bridges, and acceptors) that drive the system toward incoherent behavior at long distances. Here, we present results on a D−B−A system that addresses these issues directly.

The D−B−A system uses a series of *p*-phenylene (Ph_n) oligomers, where $n = 1-5$, to link a phenothiazine (PTZ) electron donor to a perylene-3,4:9,10-bis(dicarboximide) (PDI)[5] electron acceptor, Figure 1. Selective photoexcitation of PDI within PTZ-Ph_n-PDI results in charge separation to produce a spin-coherent singlet radical ion pair (RP), $^1(PTZ^{+\bullet}-Ph_n-PDI^{-\bullet})$, which subsequently undergoes radical pair intersystem crossing (RP−ISC) to yield $^3(PTZ^{+\bullet}-Ph_n-PDI^{-\bullet})$. The triplet RP then recombines to give almost exclusively the lowest excited triplet state of PDI (^{3*}PDI). The RP−ISC mechanism is well-known to account for triplet state formation within photosynthetic reaction centers and in selected biomimetic systems.[6−12] The rate of decay of coherent charge and spin transfer is monitored as the bridge length is increased by directly measuring the distance dependence of the spin−spin exchange interaction within the RP.[11,12] Measurements of the overall charge recombination rates at long distances show that charge transport is dominated by incoherent hopping, that is, wire-like behavior. Thus, the charge recombination mechanism changes dramatically from coherent superexchange to incoherent hopping as the bridge is lengthened. A simple model based on

(1) Parson, W. W. *Photosynth. Res.* **2003**, *76*, 81−92.
(2) Jortner, J.; Ratner, M. A. *Molecular Electronics*; Blackwell: London, 1997.
(3) Jortner, J. *J. Phys. Chem.* **1976**, *64*, 4860.
(4) Marcus, R. A.; Sutin, N. *Biochim. Biophys. Acta* **1986**, *811*, 265.
(5) Van der Boom, T.; Hayes, R. T.; Zhao, Y.; Bushard, P. J.; Weiss, E. A.; Wasielewski, M. R. *J. Am. Chem. Soc.* **2002**, *124*, 9582.
(6) Dutton, P. L.; Leigh, J. S.; Seibert, M. *Biochem. Biophys. Res. Commun.* **1972**, *46*, 406.
(7) Thurnauer, M. C.; Katz, J. J.; Norris, J. R. *Proc. Natl. Acad. Sci. U.S.A.* **1975**, *72*, 3270.
(8) Hoff, A. J. *Photochem. Photobiol.* **1986**, *43*, 727.
(9) Hasharoni, K.; Levanon, H.; Greenfield, S. R.; Gosztola, D. J.; Svec, W. A.; Wasielewski, M. R. *J. Am. Chem. Soc.* **1995**, *117*, 8055−8056.
(10) Carbonera, D.; Di Valentin, M.; Corvaja, C.; Agostini, G.; Giacometti, G.; Liddell, P. A.; Kuciauskas, D.; Moore, A. L.; Moore, T. A.; Gust, D. *J. Am. Chem. Soc.* **1998**, *120*, 4398−4405.
(11) Lukas, A. S.; Bushard, P. J.; Weiss, E. A.; Wasielewski, M. R. *J. Am. Chem. Soc.* **2003**, *125*, 3921.
(12) Weiss, E. A.; Ratner, M. A.; Wasielewski, M. R. *J. Phys. Chem. A* **2003**, *107*, 3639.

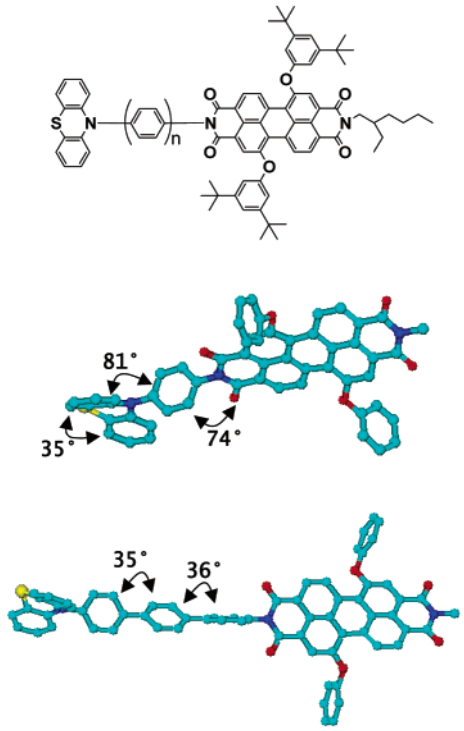

Figure 1. (A) Chemical structure of PTZ−Ph_n−PDI, where $n = 1$ for compound **1**, $n = 2$ for compound **2**, etc. (B) DFT (B3LYP, 6-31G**) energy-minimized structures for **1** and **3** with their peripheral alkyl groups and hydrogen atoms removed.

the relative energies of the RP states involved in the charge recombination process shows that charge injection into the bridge leading to wirelike transport requires a near-resonant interaction between the state in which the donor is oxidized and that in which the bridge is oxidized.

Superexchange: Coherent Charge Transport. Superexchange is thought to be an important mechanism for efficient electron transfer within the photosynthetic reaction center[13,14] and has been studied in various biomimetic systems.[15,16] The term was first used by Kramers[17] and later by Anderson[18,19] to describe the indirect exchange coupling of unpaired spins via orbitals having paired spins, which acquire paramagnetic character through mixing with charge-transfer excited-state configurations.[19] In the context of electron transfer, superexchange is the virtual mediation of charge transport from donor to acceptor via electronically well-separated bridge orbitals.

The rates of nonadiabatic electron-transfer reactions, k_{ET}, depend critically on the electronic coupling V_{DA}, whose magnitude gives the effective interaction energy between the relevant orbitals on the donor and acceptor.[3,20] When the charge-transport process originates from a state in which the redox centers are also paramagnetic, for example, charge recombination from an RP, the electronic coupling that dictates CT from the RP to energetically proximate electronic states is also that which facilitates the magnetic interaction between the unpaired spins of the RP.[17−19,21−23] Therefore, the magnitude of the magnetic interaction and its behavior as a function of donor−acceptor distance should precisely mirror that of V_{DA}.

The McConnell model for superexchange[24] predicts an approximately exponential dependence of V_{DA} on the donor−acceptor distance, r_{DA}, an assertion consistently verified by experimental data.[25−27] As the length of a bridge increases and the superexchange interaction becomes small, the rate constant for charge transfer may be dominated by the incoherent term. Incoherent or sequential charge transfer involves real intermediate states that couple to internal nuclear motions of the bridge and the surrounding medium and are therefore energetically accessible.[28] For long distances, the incoherent, wirelike channel generally becomes more efficient than the coherent one.[29,30]

Measuring the Degree of Coherent Transport using Spin−Spin Interactions. The magnetic interaction between the spins S_1 and S_2 for paramagnetic centers 1 and 2 is written in the form suggested by Heisenberg, Dirac, and Van Vleck[31]

$$H_{EX} = -2J\cdot S_1\cdot S_2 \tag{1}$$

where J is positive if the spins are parallel and negative if they are antiparallel. For two spin one-half particles, the eigenvalues of H_{EX} for $S = S_1 + S_2$ give

$$E(S) - E(S-1) = -2J\cdot S \tag{2}$$

$$E_{S-T} = E(1) - E(0) = -2J \tag{3}$$

The singlet−triplet (S−T) splitting, E_{S-T}, within the RP is therefore given by the phenomenological parameter, $2J$, the magnitude of the indirect exchange interaction.

The total spin Hamiltonian for radical pairs in solution is given by[32]

$$H_{ST} = \beta B_0(g_1S_1 + g_2S_2) + \sum_i a_{1i}S\cdot I_i + \sum_k a_{2k}S\cdot I_k + H_{EX} \tag{4}$$

where β is the Bohr magneton, B_0 is the applied magnetic field, g_1 and g_2 are the electronic g-factors for each radical, S_1 and S_2 are electron spin operators for the two radicals within the radical pair, I_i and I_k are nuclear spin operators, a_{1i} and a_{2k} are the isotropic hyperfine coupling constants of nucleus i with radical 1 and nucleus k with radical 2. For organic radicals such as those studied here, the small differences in g-factors, included in the first term of eq 4, contribute to singlet−triplet mixing only at field strengths of several Tesla, which are not relevant here. Anisotropic exchange interactions and hyperfine couplings,

(13) Marcus, R. A. *Chem. Phys. Lett.* **1987**, *133*, 471.
(14) Ogrodnik, A.; Michel-Beyerle, M.-E. *Z. Naturforsch.* **1989**, *44a*, 763.
(15) Kilsa, K.; Kajanus, J.; Macpherson, A. N.; Martensson, J.; Albisson, B. *J. Am. Chem. Soc.* **2001**, *123*, 3069.
(16) Lukas, A. S.; Bushard, P. J.; Wasielewski, M. R. *J. Phys. Chem. A* **2002**, *106*, 2074−2082.
(17) Kramers, H. A. *Physica* **1934**, *1*.
(18) Anderson, P. W. *Phys. Rev.* **1950**, *79*, 350.
(19) Anderson, P. W. *Phys. Rev.* **1959**, *115*, 2.
(20) Marcus, R. A. *J. Chem. Phys.* **1965**, *43*, 679−701.
(21) Yamashita, J.; Kondo, J. *Phys. Rev.* **1958**, *109*, 730.
(22) Miller, J. S.; Epstein, A. J.; Reiff, W. M. *Acc. Chem. Res.* **1988**, *21*, 114.
(23) Feher, O. In *Tunneling Conference*; Chance, B., Devault, D., Frauenfelder, H., Marcus, R. A., Schreiffer, J. R., Sutin, N., Eds.; Academic Press: New York, 1979; pp 729−743.
(24) McConnell, H. M. *J. Chem. Phys.* **1961**, *35*, 508.
(25) Closs, G. L.; Piotrowiak, P. J.; MacInnis, J. M.; Fleming, G. R. *J. Am. Chem. Soc.* **1988**, *110*, 2652.
(26) Roest, M. R.; Oliver, A. M.; Paddon-Row: M. N.; Verhoeven, J. W. *J. Phys. Chem. A* **1997**, *101*, 4867.
(27) Paddon-Row: M. N.; Oliver, A. M.; Warman, J. M.; Smit, K. J.; Haas, M. P.; Oevering, H.; Verhoeven, J. W. *J. Phys. Chem. A* **1988**, *92*, 6958.
(28) Nitzan, A. *Annu. Rev. Phys. Chem.* **2001**, *52*, 681.
(29) Davis, W. B.; Wasielewski, M. R.; Ratner, M. A.; Mujica, V.; Nitzan, A. *J. Phys. Chem. A* **1997**, *101*, 6158.
(30) Davis, W. B.; Svec, W. A.; Ratner, M. A.; Wasielewski, M. R. *Nature* **1998**, *396*, 60.
(31) Heisenberg, W. *Z. Phys.* **1926**, *38*, 411.
(32) Steiner, U. E.; Ulrich, T. *Chem. Rev.* **1989**, *89*, 9.

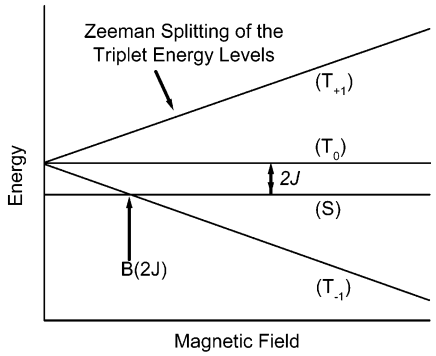

Figure 2. Schematic of radical ion pair energy levels as a function of magnetic field.

as well as the magnetic dipole−dipole interaction, are neglected because the measurements are performed in solution. Also, it is assumed that nuclei associated structurally with a given radical couple only with the electron spin within that radical.

Immediately following rapid, nonadiabatic charge separation, the correlated electron spins are in a singlet configuration. This pure state is, in general, not an eigenstate of H_{ST}, as the weakly coupled electron spins are free to precess independently around the resultant of their respective local fields (mainly because of electron−nuclear hyperfine interactions) and the external applied field. After times usually in the range of a few nanoseconds, RP−ISC results in formation of a triplet spin configuration. When hyperfine and exchange interactions are isotropic and spin−spin coupling is weak, each of the three zero-field triplet states of the radical pair will be nearly degenerate with the singlet and will be populated with equal probability at room temperature. If the spin−spin exchange interaction within the radical ion pair is nonzero, the triplet manifold is not initially degenerate with the singlet, but rather separated from the singlet by an energy 2*J*, Figure 2.

Application of a magnetic field results in Zeeman splitting of the triplet sublevels, which at high fields can be described by the T_0 and $T_{\pm1}$ states, Figure 2. In the high field limit, population of the RP triplet state occurs exclusively by $S-T_0$ mixing, while T_{-1} and T_{+1} remain unpopulated. Electron paramagnetic resonance (EPR) measurements on closely related compounds have confirmed that the triplet levels of the radical pair are higher in energy than the singlet state as would be expected from net antiferromagnetic exchange.[9] When the Zeeman energy from the applied field equals that of the S−T splitting, the low energy triplet state, T_{-1}, crosses the singlet, and the RP−ISC rate is maximized, which produces a resonance in the triplet yield at B_{2J}. An increase in the rate of triplet formation at resonance implies that the RP decay rate also increases. One can therefore monitor the RP population as a function of applied magnetic field and obtain a plot with a minimum at B_{2J} to obtain 2*J* as well.

Experimental Section

The synthesis and characterization of compounds **1**−**10** can be found in the Supporting Information. Characterization was performed with a Gemini 300 MHz, Varian 400 MHz, or INOVA 500 MHz NMR and a PE BioSystems MALDI-TOF mass spectrometer. All solvents were spectrophotometric grade or distilled prior to use.

Ground-state absorption measurements were made on a Shimadzu (UV-1601) spectrophotometer. The optical density of all samples was maintained between 0.7 and 1.0 at 532 nm ($\epsilon_{PDI,\ 550\ nm} = 46{,}000\ cm^{-1}\ M^{-1}$) for nanosecond transient absorption (TA) and between 0.3 and 0.5 at 420 nm for femtosecond TA. Redox potentials for *N*-phenylphenothiazine,[33] PDI,[34] and *p*-phenylene oligomers[35] have been obtained previously. Redox potentials obtained from these studies are listed in Table S1. Steady-state fluorescence measurements were performed on **1**−**5** and model compounds **6**−**10** and quantum yields of ^{1*}PDI fluorescence were calculated against a Rhodamine 640 standard. Quantum yields of **6**−**10** were all unity. The phenothiazine cation spectrum measured in acetonitrile[33] is characterized by a visible absorption at 510 nm, which unfortunately is undetectable in our TA experiment because of the strength of the ground-state bleach of PDI in this spectral region.

Femtosecond transient absorption measurements were made either using the 420-nm frequency-doubled output from a regeneratively amplified titanium sapphire laser system operating at 2 kHz or the 400-nm frequency-doubled output from a regeneratively amplified titanium sapphire laser system operating at 1 kHz as the excitation pulse. A white light continuum probe pulse was generated by focusing the IR fundamental into a 1-mm sapphire disk.[36] Detection with a CCD spectrograph has previously been described.[36] The samples were irradiated with 0.5−1.0 μJ per pulse focused to a 200-μm spot. Samples were placed in a 2-mm path length glass cuvette and stirred using a motorized wire stirrer to prevent thermal lensing and sample degradation. The total instrument response time for the pump−probe experiments was 150 fs. Transient absorption kinetics were fit to a sum of exponentials with a Gaussian instrument function using Levenberg−Marquardt least-squares fitting. Femtosecond transient absorption kinetic traces for compounds **1**−**3** can be found in Figure S1.

Nanosecond transient absorption measurements were made using the frequency-tripled output of a Continuum 8000 Nd:YAG laser to pump a Continuum Panther OPO. Samples were placed in a 10-mm path length quartz cuvette equipped with a vacuum adapter and subjected to five freeze−pump−thaw degassing cycles prior to transient absorption measurements. The probe light in the nanosecond experiment was generated using a xenon flashlamp (EG&G Electrooptics FX-200) and detected using a photomultiplier tube with high voltage applied to only four dynodes (Hamamatsu R928). The total instrument response time is 7 ns and is determined primarily by the laser pulse duration. Nanosecond kinetic traces for **2**, **4**, and **5** were recorded over a range of 1 μs, while those for **3** were over a range of 2 μs. Between 50 and 100 shots were averaged at each field strength with a LeCroy 9384 digital oscilloscope and sent to a microcomputer, which calculated the ΔA. Nanosecond kinetic traces for compounds **2**−**5** can be found in Figure S2. For the magnetic field effect experiment, the sample cuvette was placed between the poles of a Walker Scientific HV-4W electromagnet powered by a Walker Magnion HS-735 power supply. The field strength was measured by a Lakeshore 450 gaussmeter with a Hall effect probe. Both the electromagnet and the gaussmeter were interfaced with the data collection computer, allowing measurement and control of the magnetic field to $\pm1 \times 10^{-5}$ T during data acquisition. The magnetic field was varied by a constant increment (either 0.2 mT, 0.3 mT, 0.5 mT, 1 mT, or 5 mT depending on desired resolution). Because of the length of the sample runs (>4 h), a small amount of sample degradation was observed, resulting in a decrease in the triplet yield at zero field, $\Delta A(B = 0)$, during the experiments. To compensate for this, the magnetic field was reset to $B = 0$ mT every five kinetic traces for increments of 5 mT, every three kinetic traces for increments of 1, 0.5, and 0.3 mT, and every two kinetic traces for increments of 0.2 mT and $\Delta A(B = 0)$ was plotted and fit with a polynomial or series of polynomials. These functions were used

(33) Daub, J.; Engl, R.; Kurzawa, J.; Miller, S. E.; Schneider, S.; Stockmann, A.; Wasielewski, M. R. *J. Phys. Chem. A* **2001**, *105*, 5655.
(34) Gosztola, D.; Niemczyk, M. P.; Svec, W. B.; Lukas, A. S.; Wasielewski, M. R. *J. Phys. Chem. A* **2000**, *104*, 6545.
(35) Meerholz, K.; Heinze, J. *Electrochim. Acta* **1996**, *41*, 1839.
(36) Giaimo, J. M.; Gusev, A. V.; Wasielewski, M. R. *J. Am. Chem. Soc.* **2002**, *124*, 8530.

to calculate the relative triplet yield or RP yield as a function of applied field strength. The relative triplet yield is thus

$$\frac{T}{T_0} = \frac{\Delta A(B)}{\Delta A(B=0)}$$

with an analogous expression for the RP yield. The results presented are an average of three or more experiments conducted on separate days with freshly prepared samples in spectrophotometric or freshly distilled ACS grade toluene.

Results and Discussion

Synthesis of PTZ−Ph$_n$−PDI. The synthesis of each molecule followed a strategy in which the phenothiazine (**PTZ**) donor or the perylenediimide (**PDI**) acceptor were functionalized with a segment of the oligophenyl bridge followed by coupling of the donor- and acceptor-bearing segments. This approach avoids the solubility issues that are typically associated with (Ph$_n$) oligomers. The known 1,7-dibromoperylene-3,4:9,10-tetracarboxydianhydride was reacted with 3,5-di-*tert*-butylphenol (3 equiv) in refluxing DMF in the presence of Cs_2CO_3 (2 equiv) for 4 h. Precipitation from cold glacial acetic acid gave 1,7-diphenoxyperylene-3,4:9,10-tetracarboxydianhydride (**PDA**). The dianhydride is converted to the monoanhydride/monoimide by reacting **PDA** with 2-ethylhexylamine in refluxing pyridine for 2 h, followed by chromatographic separation of the monoimide (**PIA**) from the diimide and unreacted dianhydride, the latter two of which can be recycled.

The synthesis of **PTZ−Ph$_n$−PDI** where $n = 1$ and 2 begins by coupling 4-nitrobromobenzene or 4′-nitrobromobiphenyl to phenothiazine using Pd-catalyzed amination of the bromoarene. This yields the **PTZ−Ph$_n$−NO$_2$** ($n = 1$, 2) intermediates, both of which were subjected to $SnCl_2$/HCl reduction to afford the corresponding **PTZ−Ph$_n$−NH$_2$** ($n = 1$, 2) intermediates. Finally, condensation of the amines with **PIA** in refluxing pyridine/imidazole produced **1** and **2**. The synthesis of **PTZ−Ph$_3$−PDI**, begins with the Pd-catalyzed amination of 4′,4-dibromobiphenyl with phenothiazine using a 4-fold excess of the dibrominated starting material to avoid disubstitution. This reaction could be scaled up easily to produce large quantities of the **PTZ−Ph$_2$−Br** intermediate, which proved to be useful for later reactions. Suzuki coupling of this intermediate with 4-aminophenylboronic ester gave **PTZ−Ph$_3$−NH$_2$**. Condensation of **PTZ−Ph$_3$−NH$_2$** with **PIA** in refluxing DMF (with a catalytic amount of $ZnOAc_2$) produced **3**. The synthesis of **PTZ−Ph$_4$−PDI** starts by reacting an excess of 4,4′-dibromobiphenyl with 4-aminophenylboronic ester to give **NH$_2$−Ph$_3$−Br**. This was readily converted to the boronic ester using Pd-catalyzed cross-coupling with pinacolborane to give **NH$_2$−Ph$_3$−DB**. Because of solubility limitations, it was necessary to couple the fourth phenyl to phenothiazine first. 4-Trimethylsilylbromobenzene was aminated with phenothiazine using Pd-catalyzed cross-coupling followed by removal of the TMS with ICl to yield **PTZ−Ph−I**. Suzuki coupling of this material with the **NH$_2$−Ph$_3$−DB** intermediate produced the **PTZ−Ph$_4$−NH$_2$**, which was condensed with **PIA** in refluxing DMF (catalytic $ZnOAc_2$) to yield **4**. **PTZ−Ph$_5$−PDI** also required synthesis of the oligophenylene bridge from both "directions". First, **NH$_2$−Ph$_3$−Br** was condensed with **PIA** by refluxing in pyridine to give **PDI−Ph$_3$−Br**. The intermediate **PTZ−Ph$_2$−Br** was easily converted to the boronic ester by Pd-catalyzed cross-coupling with pinacolborane in basic p-dioxane to give **PTZ−Ph$_2$−DB**. Final Suzuki coupling of **PDI−Ph$_3$−Br** with **PTZ−Ph$_2$−DB** gave **5**. All synthetic details and characterization for compounds **1**−**10** can be found in the Supporting Information.

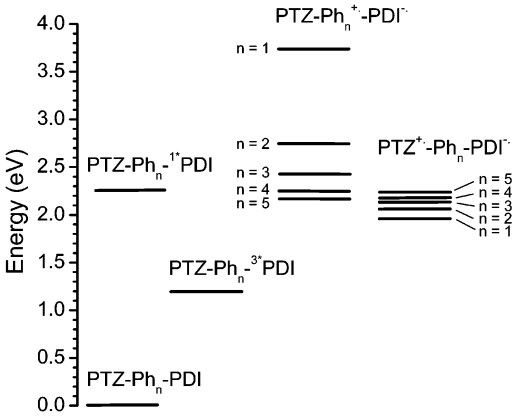

Figure 3. Energy levels for the electronic states relevant to the electron-transfer pathways for **1**−**5**.

Molecular Structures and Energy Levels. Energy-minimized structures of **1**−**5**, Figure 1, and their corresponding radical ions were calculated using density functional theory (DFT) employing Becke's three parameter hybrid functional using Lee, Yang, and Parr correlation functional (B3LYP)[37,38] and a 6-31G** basis set (please see Supporting Information for details).[39] The "pucker angle" of phenothiazine, calculated to be 147.70°, is in very good agreement with the value obtained from the X-ray structure, 146.11°.[33] PTZ and PDI are nearly perpendicular to their respective nearest-neighbor bridge units and the "twist" angle between bridge units is ∼35°. The effective distances between PTZ$^{+\bullet}$ and PDI$^{-\bullet}$ within PTZ$^{+\bullet}$−Ph$_n$−PDI$^{-\bullet}$, as well as those between Ph$_n$$^{+\bullet}$ and PDI$^{-\bullet}$ within PTZ−Ph$_n$$^{+\bullet}$−PDI$^{-\bullet}$, Table S2, are measured from the centroid of the unpaired spin distributions of PDI$^{-\bullet}$ to those of PTZ$^{+\bullet}$ and Ph$_n$$^{+\bullet}$, respectively. The spin distribution of each radical ion was obtained using the energy-minimized geometry of the radical ion, then subtracting the β spin density from the α spin density on the diagonal of the calculated spin density matrixes given by unrestricted Hartree−Fock molecular orbital calculations using the AM1 model.[40]

The energy levels for the low-lying PTZ$^{+\bullet}$−Ph$_n$−PDI$^{-\bullet}$ and PTZ−Ph$_n$$^{+\bullet}$−PDI$^{-\bullet}$ radical ion pair states within **1**−**5** are shown in Figure 3. The corresponding energies for PTZ$^{+\bullet}$−Ph$_n$$^{-\bullet}$−PDI are all very high (≥3.0 eV) and consequently will not be considered explicitly for reasons presented below. These energies were estimated using Weller's expression on the basis of the Born dielectric continuum model[41] of the solvent to determine the energy of formation of an ion pair in a solvent of arbitrary polarity:

$$E_{IP} = E_{ox} - E_{red} - \frac{e^2}{r_{DA}\epsilon_s} + e^2\left(\frac{1}{2r_1} + \frac{1}{2r_2}\right)\left(\frac{1}{\epsilon_s} - \frac{1}{\epsilon_{sp}}\right) \quad (5)$$

(37) Becke, A. D. *J. Chem. Phys.* **1993**, *98*, 1372.
(38) Lee, C.; Yang, W.; Parr, R. G. *Phys. Rev. B* **1988**, *37*, 785.
(39) *Jaguar 3.5*; Schrodinger, Inc.: Portland, Oregon, 1998.
(40) The semiempirical PM3 method implemented in HyperChem(TM) (Hypercube, Inc., 1115 NW 1114th Street, Gainesville, FL 32601).
(41) Weller, A. *Z. Phys. Chem.* **1982**, *133*, 93.

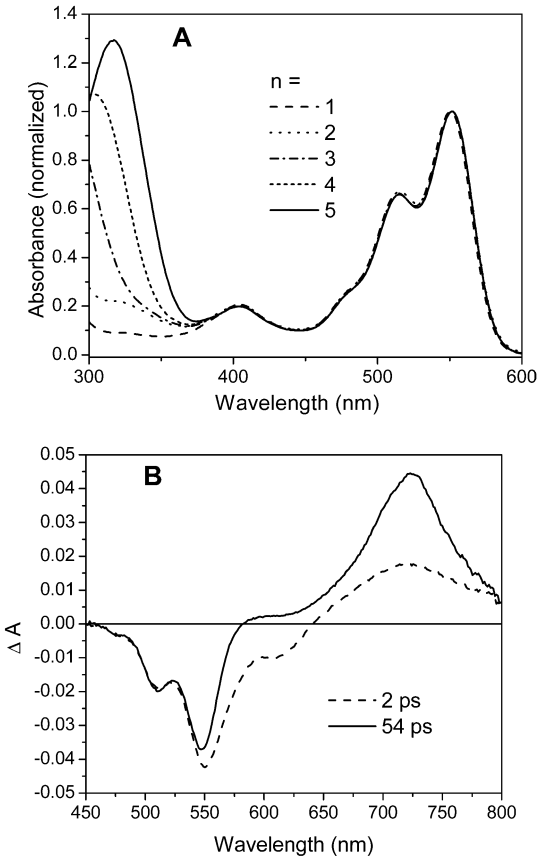

Figure 4. (A) Normalized ground-state absorption spectra of **1**−**5.** The fluorescence maxima all occur at 575 nm and the fluorescence quantum yields for **1**−**5** are, respectively, 0.03, 0.09, 0.41, 0.83, 0.89; (B) Transient absorption spectra of **1** following a 400 nm, 130 fs laser excitation pulse. The features in these spectra are indicative of the charge-separated state of the system: $PTZ^{+\bullet}-Ph-PDI^{-\bullet}$.

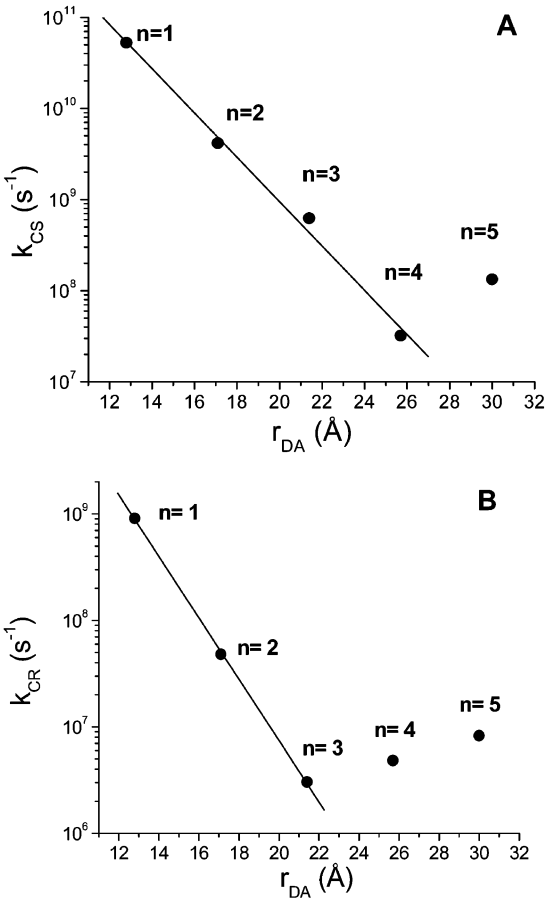

Figure 5. (A) Logarithmic plot of the charge separation rate constant, k_{CS} vs donor−acceptor distance, r_{DA}. The best fit line through the data points for $n = 1-3$ gives $R^2 = 0.98$, $\beta = 0.46$ Å^{-1}, and $k_0 = 5 \times 10^{12}$ s^{-1}. (B) Logarithmic plot of the charge recombination rate constant, k_{CR} vs donor−acceptor distance, r_{DA}. The best fit line through the data points for $n = 1-3$ gives $R^2 = 0.99$, $\beta = 0.67$ Å^{-1}, and $k_0 = 5 \times 10^{12}$ s^{-1}.

where E_{ox} and E_{red} are, respectively, the oxidation and reduction potentials of the donor and acceptor in a high polarity solvent with dielectric constant ϵ_{sp} ($\epsilon_{sp} = 25$ for butyronitrile used here), e is the charge of the electron, r_1 and r_2 are the ionic radii of the radical ions, r_{DA} is the donor−acceptor distance, and ϵ_s is the static dielectric constant of the solvent in which the spectroscopy is performed ($\epsilon_s = 2.38$ for toluene used here). Because of the well-known limitations of this treatment, the values of E_{IP} are accurate to no better than ±0.1 eV. All information used to obtain E_{IP} is given in the Supporting Information.

Spectroscopy. The ground-state spectra of compounds **1**−**5**, Figure 4A, have an absorption maximum at 550 nm, which is very similar to that of PDI alone ($\epsilon = 46\,000$ M^{-1} cm^{-1}).[5] Additionally, there is a feature between 300 and 350 nm because of Ph_n that red shifts and grows in intensity relative to the PDI peaks as n increases. Spectroelectrochemical measurements show that the ground-state absorption spectrum of $PDI^{-\bullet}$ is characterized by a strong absorption at 720 nm ($\epsilon = 79\,800$ M^{-1} cm^{-1}).[5] The transient absorption spectra of **1**−**5** following photoexcitation of PDI with 400 nm, 130 fs laser pulses display very similar features, having a broad absorption centered at 715−725 nm, a strong bleach of the ground state of PDI at 550 nm, and a band centered at 620 nm because of the stimulated emission from the lowest excited singlet state of PDI, (^{1}*PDI), Figure 4B. As ^{1}*PDI has a broad, positive absorption band centered at 720 nm which overlaps the $PDI^{-\bullet}$ feature, the decay of the stimulated emission band is the more accurate measure of charge separation rate constant within the PTZ−Ph_n−PDI systems. Since the spectroscopic signature of $PTZ^{+\bullet}$ cannot be observed because of the strong bleach of the PDI ground state, one must consider the possibility of charge separation resulting directly in $PTZ-Ph_n^{+\bullet}-PDI^{-\bullet}$ rather than $PTZ^{+\bullet}-Ph_n-PDI^{-\bullet}$. Model compounds Ph_n−PDI, where $n = 1-5$, were synthesized to test this idea. The fluorescence quantum yield of ^{1}*PDI in each molecule was unity, in contrast to the PTZ−Ph_n−PDI systems. Therefore, fluorescence of PDI is only quenched in the presence of the PTZ donor. Magnetic field effect measurements on triplet formation via the RP−ISC mechanism in PTZ−Ph_n−PDI discussed below also strongly support this conclusion.

Charge-Transport Dynamics. The distance dependence of the charge separation rate constants for **1**−**5** is monitored by the decay of the 620 nm stimulated emission feature of ^{1*}PDI, Figure 5A. For **1**−**4** these rate constants, k_{CS}, decay exponentially with donor−acceptor distance so that

$$k_{CS} = k_0 e^{-\beta(r-r_0)} \qquad (6)$$

where k_0 is the rate constant at the contact distance r_0, and $\beta = 0.46$ Å^{-1}. This strongly exponential dependence indicates that electron transfer from PTZ to ^{1*}PDI is dominated by the super-

exchange mechanism. Studies of the rates of energy transfer from $Ru(bpy)_3^{2+}$ to $Os(bpy)_3^{2+}$ through *p*-oligophenylenes via a Dexter-type (superexchange) mechanism show a similar exponential distance dependence with $\beta = 0.32$ Å^{-1}.[42] The energies of the electronic states with positive charge residing on the bridge in these molecules, PTZ−$Ph_n^{+\bullet}$−$PDI^{-\bullet}$, are high enough so that these states remain unpopulated virtual states. The data in Figure 3 show that only in **4** and **5** is the energy gap between the initial photoexcited state and the bridge RP small. The rate constant for **5** clearly does not fall on the line in Figure 5A, so that electron transfer through Ph_5 may be on the threshold of a change in electron-transfer mechanism to incoherent hopping.

The rate constants for charge recombination in **1**−**5** are obtained from the decay rate of $PDI^{-\bullet}$, Figure 5B, kinetic traces in Figures S1 and S2. Charge recombination within compounds **1**−**3** is strongly exponential, and the plot of log(k_{CR}) versus r_{DA} yields $\beta = 0.67$ Å^{-1}. The rate constants for charge recombination in **4** and **5**, however, do not lie along the linear curve established by **1**−**3**, and, in fact, actually *increase* with increasing bridge length. For charge recombination within these compounds, a switch in mechanism from superexchange to thermally activated hopping is postulated as the bridge is lengthened.

A change in charge recombination mechanism from superexchange to hopping relies on efficient charge injection into the Ph_n bridge such that the PTZ$^{+\bullet}$−$Ph_n^{-\bullet}$−PDI or PTZ−Ph_n^{+}−$PDI^{-\bullet}$ states are real intermediates. The energies of PTZ$^{+\bullet}$−$Ph_n^{-\bullet}$−PDI for $n = 1-5$ all are ≥3.0 eV, so that electron injection onto the bridge during the charge recombination reaction cannot occur. On the other hand, as the bridge lengthens, the calculated energy of PTZ−$Ph_n^{+\bullet}$−$PDI^{-\bullet}$ decreases significantly because of the increased conjugation length, as can be seen in the decrease in oligophenylene band gap energy from 7.3 eV for $n = 1$ to 3.3 eV for $n = 5$, as calculated with time-dependent DFT (B3LYP hybrid functional, 6-31G** basis set) using the Q-Chem 2.1 software package.[43] The accompanying increased ease of oxidation of the oligo-*p*-phenylene, coupled with the increase in the energy of PTZ$^{+\bullet}$−Ph_n−$PDI^{-\bullet}$ largely because of Coulomb destabilization, Figure 3, leads to a near resonance of PTZ−$Ph_n^{+\bullet}$−$PDI^{-\bullet}$ with PTZ$^{+\bullet}$−Ph_n−$PDI^{-\bullet}$ for $n = 4$ and 5. The slight increase in charge recombination rate observed for **4** and **5**, relative to **3**, may be due to the combination of the increasing electronic interaction between PTZ$^{+\bullet}$−Ph_n−$PDI^{-\bullet}$ and PTZ−$Ph_n^{+\bullet}$−$PDI^{-\bullet}$ as the energy gap between them becomes smaller and the decreasing internal reorganization energy associated with putting a charge on a longer bridge.

The RP states, PTZ$^{+\bullet}$−Ph_n−$PDI^{-\bullet}$, may of course recombine either from the singlet or triplet RP state, but several observations suggest that the rate of charge recombination from the triplet RP, ^{3}(PTZ$^{+\bullet}$−Ph_n−$PDI^{-\bullet}$) → PTZ−Ph_n−^{3*}PDI, is much faster than the corresponding rate from the singlet RP to the singlet ground state, ^{1}(PTZ$^{+\bullet}$−Ph_n−$PDI^{-\bullet}$) → PTZ−Ph_n−PDI, Figure 3. First, the recombination rates of compounds **2**−**5** are markedly single-exponential despite the fact that there are two possible recombination pathways. Second, ^{3*}PDI formation, monitored at 480 nm, occurred with nearly the same rate constant as $PDI^{-\bullet}$ decay in compounds **2**−**4**. In **5**, the rise of the triplet is obscured by a strong negative feature due to ^{1*}PDI fluorescence, which makes the kinetic trace difficult to fit. Third, the RP yield of compounds **3**−**5,** (see Figure 6B for data on 4) reaches a minimum at $B = B_{2J}$, where RP−ISC is most efficient. Therefore, the RP is decaying most efficiently when the most triplet RP is being produced, indicating that the triplet recombination pathway is significantly faster than the singlet pathway. The reason for the dominance of the triplet pathway is that the free energies for singlet charge recombination in **1**−**5**, where $-\Delta G_{CR} = 2.0-2.3$ eV, are much deeper within the Marcus inverted region of the rate versus free energy of reaction profile,[20] that is, $|\Delta G| > \lambda$, where λ is the total reorganization energy for charge recombination (∼0.6 eV for these systems, please see the Supporting Information), than the corresponding free energies for triplet charge recombination, where $-\Delta G_{CR} = 0.8-1.1$ eV.

Magnetic Field Effects. Figure 6A, B shows a plot of ^{3*}PDI yield following RP recombination within **2** (A) and **3** (B) as a function of applied magnetic field, while Figure 6C, D shows a similar plot of the RP yield for **4** (C) and **5** (D). The maximum of the triplet yield plot (and minimum of the RP yield plot) marks the field at which the S and T_{-1} levels of the RP cross, resulting in maximum triplet production. This field then corresponds to the energy 2*J*, the zero-field splitting of the singlet and triplet RP levels because of magnetic superexchange coupling. Figure 7 shows a clear exponential decrease of 2*J* with r_{DA} for **2**−**5**, providing strong evidence that the charges recombining through the RP−ISC mechanism are localized on the donor and acceptor and not somewhere on the bridge. The value of 2*J* cannot be measured for compound **1** because the RP does not live long enough for RP−ISC to produce adequate yields of ^{3*}PDI to observe.

The singlet and triplet RP states are either stabilized or destabilized through one- and two-step virtual charge transfers via coupling of the orbitals on the paramagnetic centers to the bridge orbitals and to each other. The total perturbation to each RP state, ΔE_S or ΔE_T for the singlet and triplet, respectively, is a sum of pairwise interactions between the RP state and the state to which it couples via charge transfer. By simple second-order perturbation theory,

$$2J = \Delta E_S - \Delta E_T = \left[\sum_n \frac{|\langle \Psi_{RP}|V_{RP-n}|\Psi_n\rangle|^2}{E_{RP} - E_n - \lambda}\right]_S - \left[\sum_n \frac{|\langle \Psi_{RP}|V_{RP-n}|\Psi_n\rangle|^2}{E_{RP} - E_n - \lambda}\right]_T \quad (7)$$

where the indicated matrix elements couple the singlet and triplet RP states to states *n*, E_{RP} and E_n are energies of these states, respectively, and λ is the total nuclear reorganization energy of the charge-transfer reaction.[19] In principle, eq 7 can be used to determine the matrix elements for these interactions given that 2*J* has been determined experimentally for **2**−**5**, E_n can be obtained from the optical absorption and emission spectra of the excited states, the Weller equation can be used to estimate E_{RP}, and the dielectric continuum model of solvation and electronic structure methods can be used to calculate λ. However, not all contributing states are observable spectroscopically, and the errors involved in estimating the energy denominators in eq 7 are far greater than the measured values of 2*J*,

(42) Schlicke, B.; Belser, P.; De Cola, L.; Sabbioni, E.; Balzani, V. *J. Am. Chem. Soc.* **1999**, *121*, 4207−4214.
(43) *Q-Chem 2.1*; Q.-C. I.: Pittsburgh, PA, 1998.

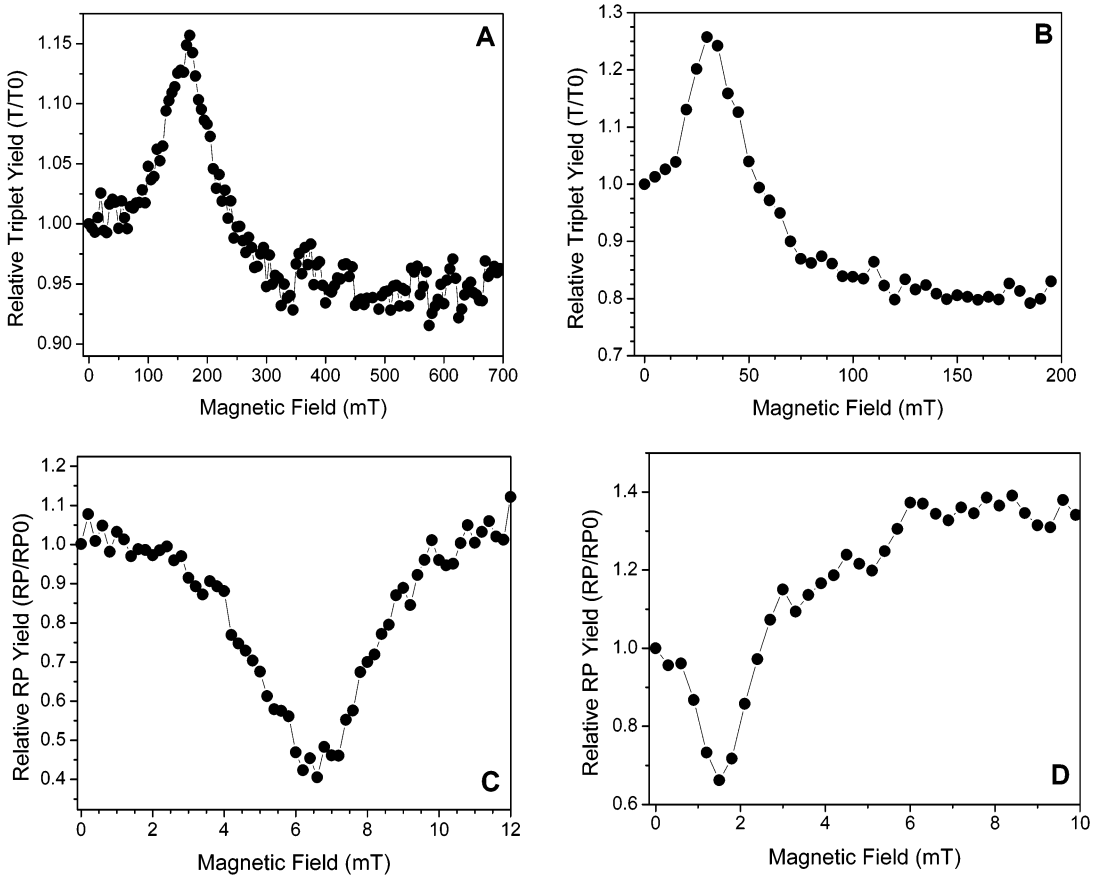

Figure 6. (A) Plot of the relative yield of ^{3*}PDI vs magnetic field strength for PTZ−Ph_2−PDI ($2J$ = 170 mT, A) and PTZ−Ph_3−PDI ($2J$ = 31 mT, (B) plot of the relative radical ion pair yield vs magnetic field strength for PTZ−Ph_4−PDI ($2J$ = 6.4 mT, C) and PTZ−Ph_5−PDI ($2J$ = 1.5 mT, D).

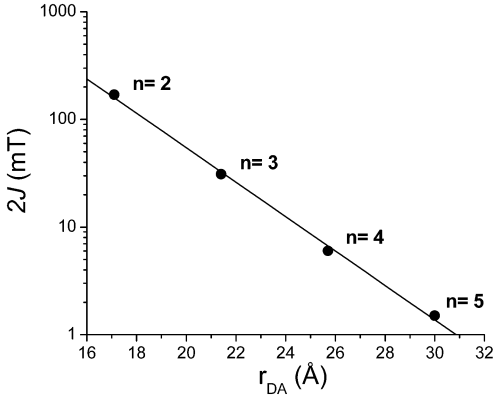

Figure 7. Logarithmic plot of the spin−spin exchange interaction, $2J$ vs r_{DA}. The best fit line through the data points for $n = 2-5$ gives $R^2 = 0.99$ and a slope of -0.37 Å^{-1}.

which are about $10^{-5}-10^{-7}$ eV. In addition, for singlet−triplet splittings of such small magnitude, there may be significant contributions from direct exchange terms that we are not considering here.[21,22,44] This is clearly a case where experiment is far more accurate than quantitative theory at this time.

As in studies concerning couplings between paramagnetic metal centers[45−47] and biradicals,[48−51] multiple CT pathways ($\sigma-\sigma$, $\sigma-\pi$, $\pi-\pi$) may be contributing to the S−T splitting, but $2J$ clearly depends exponentially on r_{DA} within this series (β = 0.37 Å^{-1}). Previous work in calculating $2J$ has shown[44] that assigning different distance dependencies to different CT pathways in hopes of distinguishing the respective orbitals involved does not improve the fit to experimental data over using a single exponential. Although we may not now be able to deconvolute the separate contributions of various CT pathways to the total S−T splitting, the $2J$ measurement is, in itself, directly related to donor−acceptor coupling, which is also inherently a sum of many electron-transfer processes. The exponential decrease of $2J$ with r_{DA} parallels the approximately exponential decay of the coherent contribution to the various ET processes. An increase in CR rate for **4** and **5** must therefore be due to the dominance of an incoherent CT channel, namely, a hopping process. As stated previously, however, the magnitude of $2J$ depends only on contributions from virtual excitations from the charge-separated state, so the path that the electron takes to get from donor to acceptor (whether it be real occupation of the bridge or superexchange) is actually irrelevant in determining $2J$. It is true that, as the bridge is lengthened, the changing energy level configuration promotes increased mixing with the bridge-occupied state, but at the cost of mixing with other configurations, and thus, as the distance between the

(44) Weihe, H.; Guedel, H. U. *J. Am. Chem. Soc.* **1997**, *119*, 6539.
(45) Pardo, E.; Faus, J.; Julve, M.; Lloret, F.; Munoz, M. C.; Cano, J.; Ottenwaelder, X.; Journaux, Y.; Carrasco, R.; Blay, G.; Fernandez, I.; Ruiz-Garcia, R. *J. Am. Chem. Soc.* **2003**, *125*, 10770−10771.
(46) Brunold, T. C.; Gamelin, D. R.; Solomon, E. I. *J. Am. Chem. Soc.* **2000**, *122*, 8511−8523.
(47) McCleverty, J. A.; Ward, M. D. *Acc. Chem. Res.* **1998**, *31*, 842−851.
(48) Closs, G. L.; Forbes, M. D. E.; Piotrowiak, P. J. *J. Am. Chem. Soc.* **1992**, *114*, 3285.
(49) Staerk, H.; Kuehnle, W.; Treichel, R.; Weller, A. *Chem. Phys. Lett.* **1985**, *118*, 19−24.
(50) Staerk, H.; Busmann, H.-G.; Kuhnle, W.; Treichel, R. *J. Phys. Chem.* **1991**, *95*, 1906.
(51) Shultz, D. A. *Comments Inorg. Chem.* **2002**, *23*, 1−21.

two spins decreases, so does the overall magnitude of their magnetic interaction.

Conclusions

The oligomeric *p*-phenylene bridge acts as a molecular wire for the charge recombination reaction of $PTZ^{+\bullet}-Ph_n-PDI^{-\bullet}$ when $n \geq 4$. Charge recombination can occur via two distinct pathways involving RP intermediates with singlet and triplet spin configurations. Direct measurement of the singlet−triplet splitting, $2J$, within the RP, using the magnetic field dependence of the RP and triplet product yields, provides quantitative evidence that the magnetic superexchange coupling, and therefore the probability of a coherent electron transfer mechanism, decreases approximately exponentially as the bridge lengthens. Concurrently, the near resonant interaction of $PTZ^{+\bullet}-Ph_n-PDI^{-\bullet}$ and $PTZ-Ph_n{}^{+\bullet}-PDI^{-\bullet}$, when $n = 4$ and 5, makes incoherent hopping a viable charge-transfer mechanism. These two effects combine to ensure the dominance of wirelike charge transport for **4** and **5**. Our results allow us to observe for the first time the relative contributions of both the coherent superexchange and incoherent hopping mechanisms to the overall charge transport process in a conjugated bridge molecule.

Acknowledgment. M.R.W. acknowledges support by the Division of Chemical Sciences, Office of Basic Energy Sciences, U.S. Department of Energy under grant no. DE-FG02-99ER-14999. M.A.R. acknowledges support from MRSEC sponsored at Northwestern by the National Science Foundation, and the MURI/DURINT program of the DOD. E.A.W. acknowledges a Fellowship from the Link Energy Foundation. We thank A. Burin, Igor Kurnikov, and A. Troisi for useful discussions.

Supporting Information Available: Experimental details regarding the synthesis and characterization of molecules used in this study, as well as additional transient kinetic and electrochemical data (PDF). This material is available free of charge via the Internet at http://pubs.acs.org.

JA0398215